Cosmic-ray diffusion in a sectored magnetic field in the distant heliosheath

V. Florinski[1,2], F. Alouani-Bibi[2], J. Kota[3], and X. Guo[2]

Received _____; accepted _____

[1]Department of Physics, University of Alabama, Huntsville, AL 35899

[2]Center for Space Plasma and Aeronomic Research, University of Alabama, Huntsville, AL 35899

[3]Lunar and Planetary Laboratory, University of Arizona, Tucson, AZ 85721

ABSTRACT

Very high intensities of galactic cosmic rays measured by Voyager 1 in the heliosheath appear to be incompatible with the presence of a modulation "wall" near the heliopause produced by a pile up of the heliospheric magnetic field. We propose that the modulation wall is a structure permeable to cosmic rays as a result of a sectored magnetic field topology compressed by plasma slowdown on approach to the heliopause and stretched to high latitudes by latitudinal flows in the heliosheath. The tightly folded warped current sheet permits efficient cosmic-ray transport in the radial direction via a drift-like mechanism. We show that when stochastic variations in the sector widths are taken into account, particle transport becomes predominantly diffusive both along and across the magnetic sectors. Using a test-particle model for cosmic rays in the heliosheath we investigate the dependence of the diffusion coefficients on the properties of the sector structure and on particle energy.

Subject headings: cosmic rays — magnetic fields — turbulence — solar wind

1. Introduction

The twin Voyager space probes are currently exploring the distant heliosheath region and are expected to reach the heliospheric boundary, known as the heliopause, and pass into the surrounding interstellar space before the end of the decade. Before crossing the heliopause, the Voyagers are expected to enter a region of rapidly changing magnetic field which is a remnant of magnetic sectors separated by an oscillating heliospheric current sheet (HCS). From global heliospheric simulations reported by Czechowski et al. (2010), Borovikov et al. (2011), and Florinski (2011), it emerges that sectors become narrower as the solar wind plasma slows down as it nears the heliopause. It was suggested by Florinski (2011) that highly energetic charged particles, such as galactic cosmic ray ions, will be profoundly affected by the compressed sector structure in the heliosheath. Charged particles find it much easier to travel across the sectors, and hence across the magnetic field, when the width of a sector is comparable to or smaller than their Larmor radius (rather than being much larger than the latter, as is typically the case in the solar wind). The enhanced cross-field transport process is a consequence of fast drift-like motion across the stack of magnetic sectors.

Voyager observations (Burlaga et al. 2003) show no regular magnetic sector pattern in the distant solar wind, a trend that appears to persist into the heliosheath (Burlaga & Ness 2010). Measured sector durations in the solar wind were, on average, shorter than 13 days expected from a simple two-sector pattern implying a significant distortion of the shape of the HCS. The widths of magnetic sectors reported by Burlaga et al. (2003) varied by almost a factor of 10 and had a sufficiently broad distribution.

Burlaga et al. (2003) only reported sectors observed during three years near the maximum of solar activity. Close to solar minima magnetic sectors occupy only a narrow range of heliolatitudes. They were not observed by the Voyagers during the pre-termination

shock part of the mission when the spacecraft was above (V1) or below (V2) the current sheet. The situation changes dramatically in the heliosheath. Here the flow is deflected away from the radial direction (Richardson et al. 2009) stretching the HCS in latitude and longitude (Czechowski et al. 2010; Borovikov et al. 2011). In the hemisphere facing the interstellar flow the sector structure is expected to exist at all latitudes deep into the heliosheath. It is then of great importance to understand the effect of the tightly folded current sheet on energetic particles, such as galactic cosmic rays.

It was proposed in Florinski (2011) that variability in sector width results in an enhanced cross-field diffusion of galactic cosmic rays with a Larmor radius greater than about 0.1 AU. The process could well be responsible for very high intensities of galactic helium ions measured by Voyager 1, intensities that are presently (2011–2012) near or in excess of the predicted interstellar values (Webber & Higbie 2009). Florinski (2011) used a simple, one-dimensional sector model that did not take into account variations in the shape of current sheets. The present paper reports a much more complete, two-dimensional model of particle transport near a rapidly oscillating HCS. Here we assume that the sector width in the distant heliosheath varies about a well defined mean, and that the variation occurs as a result of differential (variable in latitude) current sheet displacement in the radial direction. This work therefore builds upon the ideas proposed in Florinski (2011) to develop a *quantitative* model of cosmic-ray transport in a sectored magnetic field of the distant heliosheath.

It is noteworthy that a partially related concept was proposed much earlier as a mechanism of interstellar dust grain transport in the solar wind (Morfill & Grün 1979; Czechowski & Mann 2003). High rigidity and small velocity of dust grains makes their transport qualitatively different from that of cosmic rays. Dust particles larger than about 0.01 μm have gyroradii comparable to the size of the heliosphere and their trajectories

are only mildly perturbed by the sector structure in the solar wind. These slowly moving particles acquire a velocity component perpendicular to the interplanetary magnetic field and parallel to the sectors as a result of the motional electric field in the frame of the particle. Random variations in sector duration then lead to a diffusion in pitch angle. For galactic cosmic rays with their high velocities this effect is negligible, and the principal mode of transport is drift associated with the current sheet crossings.

The paper is structured as follows. In Section 2 we discuss the fundamental physics of particle drift in a sectored magnetic field. In section 3 we investigate cosmic ray transport through a stack of magnetic sectors with a test-particle orbit integration method commonly used to simulate scattering and cross-field transport in turbulent magnetic fields (e.g., Giacalone & Jokipii 1999; Mace et al. 2000; Qin et al. 2002). We demonstrate that particle transport in a magnetic field composed of variable-width sectors of alternating polarity is diffusive both parallel to and across the current sheets. The results from this study are reported in Section 4. These results reveal the dependence of the diffusion coefficients on the distribution of sector widths and on the cosmic-ray energy. Finally, Section 5 explores some consequences of the new diffusion mechanism for cosmic-ray propagation through the heliosheath.

2. Neutral sheet diffusion as a drift process

Consider an energetic charged particle, such as a galactic cosmic ray ion placed in a magnetic field that has the same magnitude everywhere, but can change sign. A change of sign occurs across a neutral sheet with negligible thickness (i.e., thickness much smaller than the Larmor radius of the energetic particle). It is well known that in the absence of a large-scale plasma flow, the particle can either gyrate in place (ignoring the motion along the magnetic field, which is of no interest here), or undergo a meandering motion (drift)

along a single current sheet. When the sectors become squeezed together, as one expects will happen on approach to the heliopause, the distance between adjacent neutral sheet folds would become comparable or smaller than the cosmic ray cyclotron radius r_g, which is typically between 0.05 and 0.3 AU in the heliosheath.

The slowly moving heliosheath plasma is thought to be nearly incompressible, which appears to be consistent with Voyager 2 results (Richardson & Wang 2011). The plasma is therefore not compressed, but follows different paths toward the tail (spreads out in latitude and longitude). Evidently, for primarily north-south flows the magnitude of the mean field need not increase because the decrease in the radial distance between field lines (as the sectors become thinner) is balanced by spreading of the field lines in latitude. For azimuthal flows, the magnitude of **B** should increase because in that case plasma follows magnetic field lines. Altogether, we expect the magnetic field to increase by a modest amount, so that the ratio of r_g to the mean distance between sectors d increases with heliocentric distance. At some distance, therefore, the critical condition $2r_g = d$ will be satisfied.

To support our estimate we calculated the magnetic field and the mean sector width in the heliosheath as a function of radial distance from the Sun using a three-dimensional model of the heliosphere that includes neutral hydrogen atoms (Florinski 2011). From this data we calculated the Larmor radius r_g for 20, 200, and 2000 MeV/n He^{2+} ions as a function of heliocentric distance. Figure 1 shows the radial dependence of d and $2r_g$ in the upwind (nose) direction. Because of its blunt shape, the termination shock stand-off distance, marked by the dotted line, is smaller ($\sim$ 74 AU) than in the directions of Voyager 1 and 2. The model is steady-state and does not include dynamic solar wind structures, but is sufficient to illustrate our point. Readers interested in the model boundary conditions for the solar wind and the local interstellar medium are referred to Florinski (2011).

From the figure, the gyro-radius does decrease with distance, but not as rapidly as

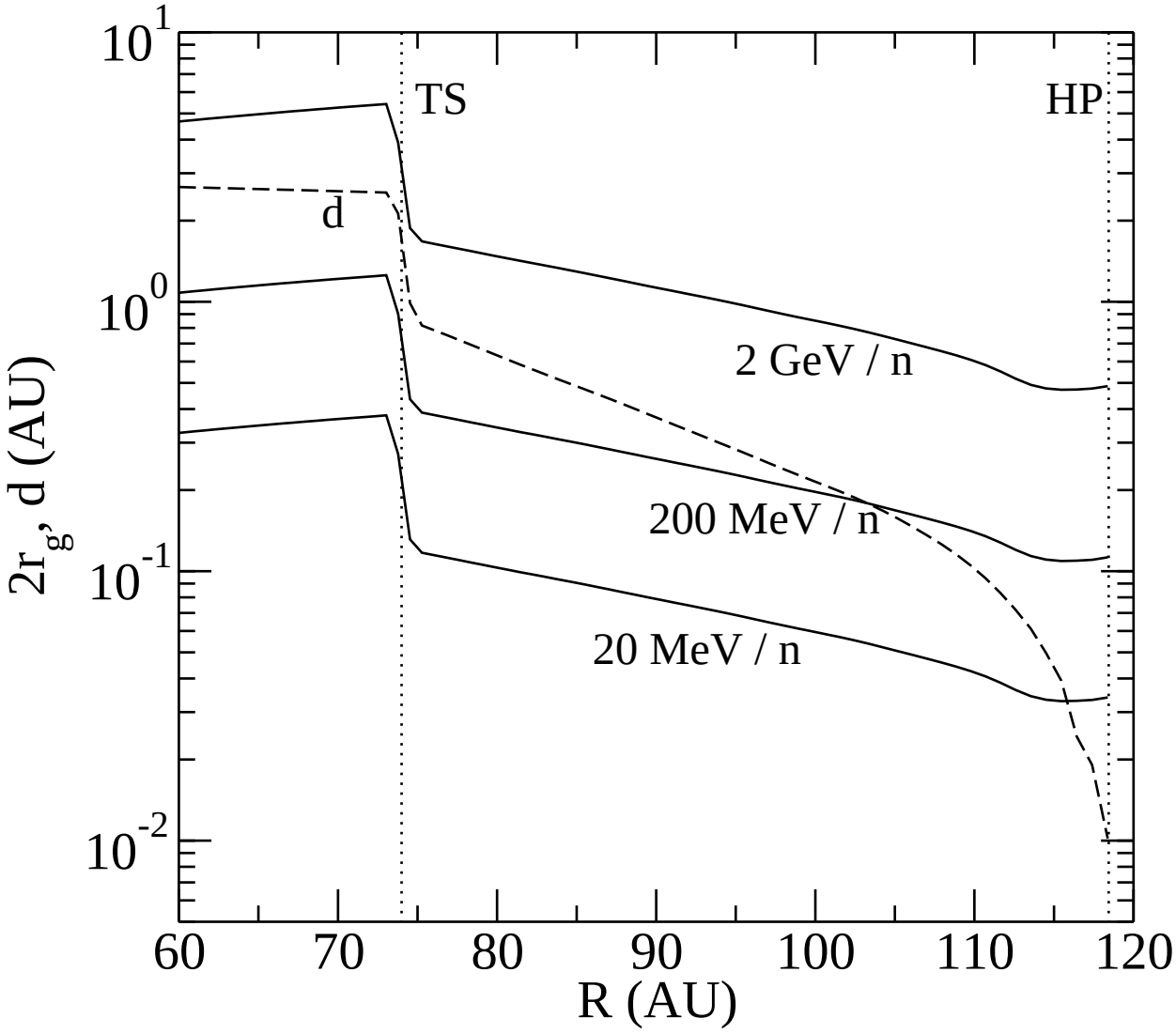

Fig. 1.— Larmor radius of galactic helium at three different energies per nucleon (solid lines) and the mean thickness of a magnetic sector in the heliosheath in the upwind (nose) direction. Current sheet diffusion is expected to be important between the intersection point of the $2r_g$ and d curves and the heliopause. The positions of the termination shock and the heliopause are marked with dotted lines.

the sector width. In the model the magnetic field magnitude increases from 0.15 nT to 0.5 nT between the termination shock and the heliopause, whereas the sector width decreases by nearly two orders of magnitude. The point of intersection between the solid and the dashed curves in Figure 1 ($2r_g = d$) gives the approximate distance beyond which the effects of neutral shift diffusion become noticeable. For 200 MeV/n ions this occurs about two-thirds of the way through, but only close to the heliopause for 20 MeV/n and lower energy particles.

As discussed in Florinski (2011), for $r_g \leq d/2$ there exist gyrophase angles for which meandering or gyrating particles are unable to complete their cycle before encountering a neighboring current sheet. At that point the particle's sense of rotation will change as its guiding center "jumps" across the sheet and into an adjacent sector. Figure 2 shows a typical trajectory of an energetic particle in an ensemble of sectors of uniform width. The particle drifts in both y and x directions. However, unlike the former drift, it is easy to see by drawing a similar diagram for a different starting gyrophase, that drift across the magnetic boundaries can proceed in either direction (to the left or to the right on the figure, depending on the gyrophase). It follows that the net drift velocity is zero for a gyrotropic ensemble of particles. However, the process itself may lead to a separation of an initially symmetric distribution into left- and right-going components.

Despite the limitation, the drift process discussed above could enhance the *diffusive* transport of energetic particles if the sector structure is not uniform. Observations clearly show that the sector widths (or duration, in terms of spacecraft measurements) vary by a factor of ~ 10 in the outer heliosphere (Burlaga et al. 2003). This variability is presumably due to both an irregular magnetic field structure on the Sun and the dynamic interaction between structures in the solar wind further distorting the shape of the HCS (e.g. Riley et al. 2002; Intriligator et al. 2005). One expects the sector thickness to vary with

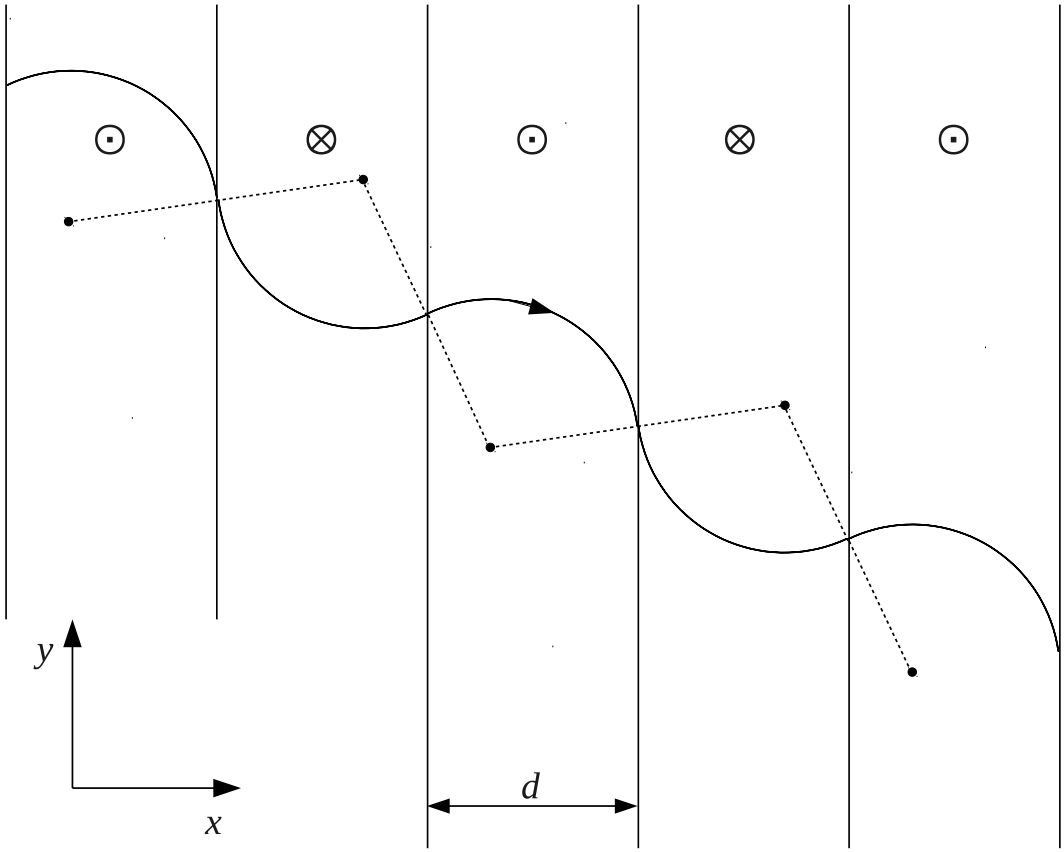

Fig. 2.— Drift motion of a positively charged ion through a stack of magnetic sectors of alternating polarity. The solid line is the particle's trajectory and the dotted line shows the "trajectory" of its guiding center. The magnetic field is in and out of the plane of the figure.

both latitude and longitude; we include only latitudinal variations in our two-dimensional model (see below). The advantage of the present model is simplicity stemming from the assumption that the magnetic field varies in direction only, but not in magnitude (this condition cannot be maintained in the fully three-dimensional case). This allows us to focus on the fundamental physics of the diffusion process due to current sheet fluctuations, a feature that would otherwise be hidden underneath the complexity of a fully 3D simulation.

In the last part of this section we present a simple two-dimensional model, based on the Boltzmann equation, that illustrates the qualitative features expected from closely packed alternating sectors. In this model, the sector width is fixed and the randomness is provided by scattering centers embedded in the plasma. For the sake of brevity, we consider only the motion in the xy plane (with the background magnetic field directed along $\hat{\mathbf{z}}$), and disregard scattering in pitch angle, which would lead to quantitative modifications but would not change the robust qualitative features. We assume the pitch angle to be $\pi/2$ and consider scattering in gyrophase angle φ only.

As in Figure 2 we take the distribution function of cosmic rays to be independent of y. Assuming that diffusion is a result of independent small-angle scattering in φ, the Boltzmann equation for the phase space density $f(x, \varphi, t)$ can be written as

$$\frac{\partial f}{\partial t} + v \cos\varphi \frac{\partial f}{\partial x} - \Omega \frac{\partial f}{\partial \varphi} = \frac{\partial}{\partial \varphi}\left(\frac{1}{\tau}\frac{\partial f}{\partial \varphi}\right), \tag{1}$$

where $\Omega = v/r_g$ is the gyro-frequency and τ is the mean scattering time. The velocity v is the same for all particles. Physically, τ^{-1} is related to the quasi-linear Fokker-Planck coefficient $D_{\varphi\varphi}$ that describes diffusion in gyrophase through resonant interactions with turbulent magnetic fields (Achatz et al. 1991). The latter is a function of pitch-angle cosine μ and velocity v; since both are constant in our model, we accordingly take $\tau = \text{const}$.

For a unipolar field pointing in the $\hat{\mathbf{z}}$ direction (i.e. constant Ω), Eq. (1) entertains the

following steady-state solution

$$f(x,\varphi) = F_0 + G_x x + \frac{2S_x^0}{v}\cos\varphi + \frac{2S_y^0}{v}\sin\varphi, \tag{2}$$

implying that a steady gradient (G_x) produces streaming $S_{x,y}^0 = (2\pi)^{-1}\int f v_{x,y} d\varphi = -\kappa_{(x,y)x} G_x$ in the $\hat{\mathbf{x}}$ and $\hat{\mathbf{y}}$ directions, respectively, consistently with the nominal diffusion coefficients of $\kappa_{xx} = v^2\tau/[2(1+\Omega^2\tau^2)]$ and $\kappa_{yx} = -\Omega\tau\kappa_{xx}$.

Next, we place alternating sectors of widths d_+ and d_- periodically in the yz plane. Though the solution shown in Eq. (2) remains formally a solution, one should bear in mind that S_y now becomes discontinuous at the current sheets, while the physical solution must be continuous. We note that an approach based on Parker's equation (Parker 1965) cannot be directly applied near current sheets because Parker's equation does not include shear. Its extension to include second-order terms shows that shear produces significant higher harmonics (Kota 1975; Earl et al. 1988), which cannot be neglected in our case.

To represent a large scale gradient, G_x, we assume a solution of the Boltzmann equation (1) in the form:

$$f(x,\varphi) = G_x x + F(x,\varphi), \tag{3}$$

where $F(x,\varphi)$ is periodic in x and is required to be continuous at the currents sheets. Integrating Eq. (1) immediately yields a physically plausible result that streaming in the x direction, S_x, must be constant. The ratio of the computed S_x/G_x represents the effective diffusion coefficient appropriate to this situation. We solve Eq. (1) numerically on a 200×120 grid in x and φ. Numerical results presented here were all obtained with $\lambda = 5r_g$ (i.e., $\Omega\tau = 5$). Furthermore, we consider a symmetric arrangement with $d_+ = d_- = D/2$, as well as an asymmetric one with a dominant sector by choosing $d_+ = 3D/4$ and $d_- = D/4$.

Figure 3 shows how the streaming S_x changes if the sectors become narrower, i.e., r_g/D increases. Because $S_x \sim \kappa_{xx}$ (assuming a constant spatial gradient), the figure also

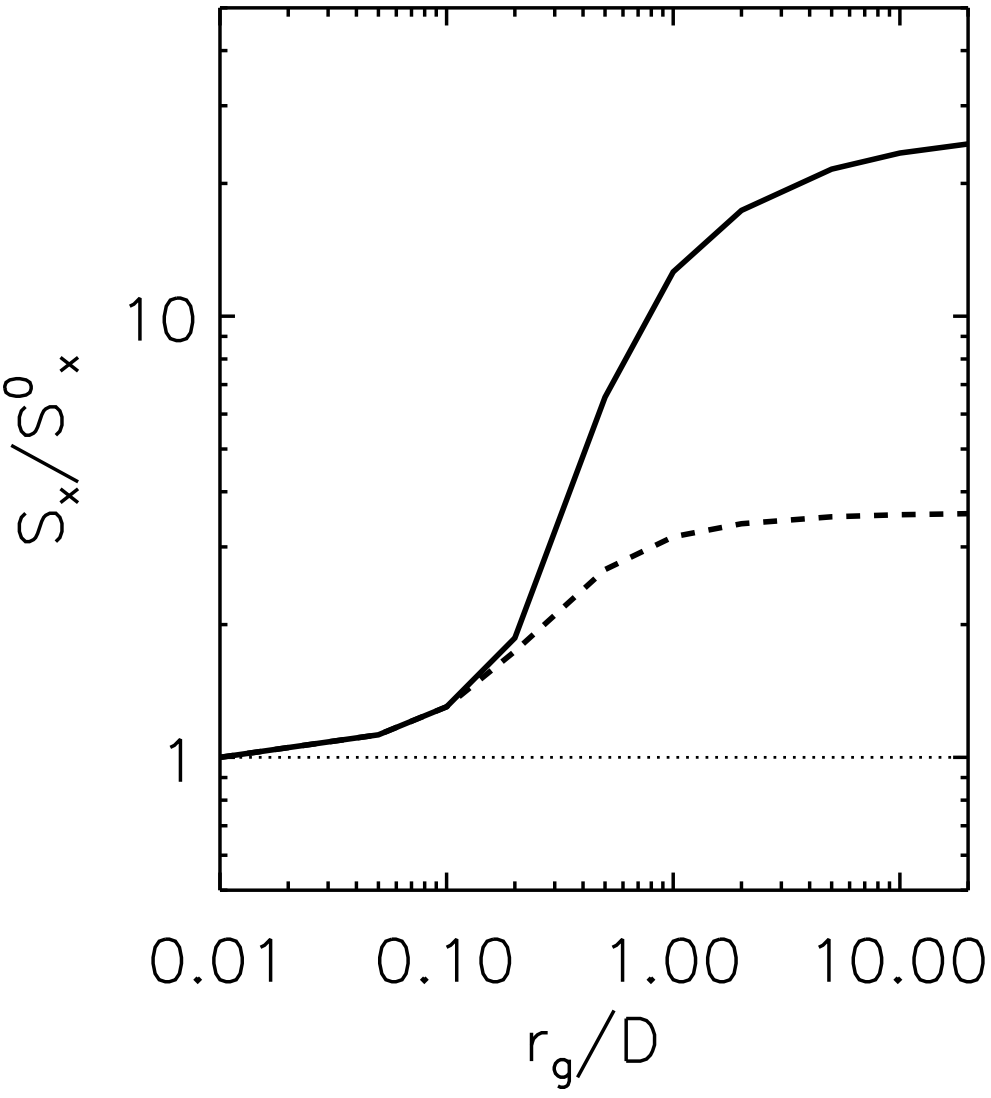

Fig. 3.— The increase of the streaming S_x in the x direction relative to the nominal streaming obtained for a uniform field. The solid curve refers to equidistant alternating sectors, the dashed curve refers to an asymmetric case with a dominant sector (see text).

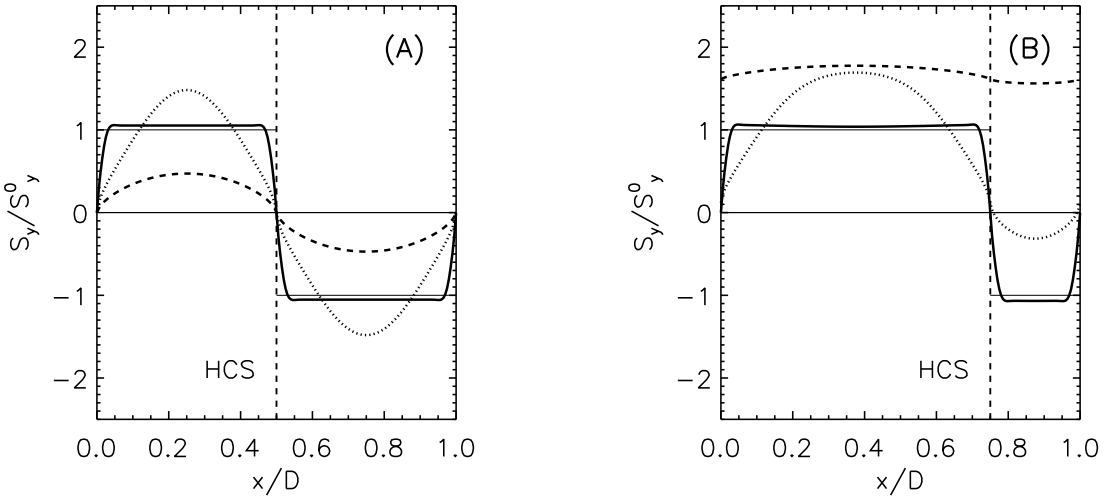

Fig. 4.— Spatial variation of the diffusive streaming S_y (solid: $r_g/D = 0.02$, dotted: $r_g/D = 0.2$, dashed: $r_g/D = 2$). While $S_y(x)$ has a sharp transition at the HCS for $r_g/D \ll 1$, it decreases in magnitude as r_g/D increases. The left panel shows a symmetric case with two equally wide sectors, the right panel shows the asymmetric arrangement with a dominant sector (see text). Note that S_y remains large in the latter case.

shows the ratio between the cross-field diffusion coefficients with and without the sectors. The two curves refer to the symmetric and asymmetric arrangements, respectively. Clearly, particle transport is significantly faster as the thickness of the sectors becomes comparable or smaller than the particle's gyro-radius, r_g. The increase is larger in the symmetric case, when S_x approaches the limiting case obtained without any background field ($\Omega = 0$), which is about a 25-fold increase for our parameters ($\Omega\tau = 5$). For the asymmetric case the increase is slower. Intuitively one can see that particles will sense the average Ω, which implies a twofold decrease in $\langle\Omega\rangle$, and a corresponding fourfold increase in S_x relative to the unipolar case.

Figure 4 illustrates the spatial variation of the S_y streaming component for the values of $r_g/D = 0.02$, $r_g/D = 0.2$, and $r_g/D = 2$ within a single pair of sectors (the complete solution is of course periodic in x). For small r_g/D the solution is close to the formal discontinuous solution, with a sharp transition occurring near the current sheet. We note that the directional distribution has significant higher order anisotropies in this region. S_y decreases as r_g/D increases. The right panel of Figure 4 shows the asymmetric case, with one sector dominating. This case yields a remarkably large streaming in the y-direction in both sectors for $r_g/D = 0.2$. This seemingly counter-intuitive result can be readily understood recalling that multiplying Eq. (1) by $\sin\varphi$ and averaging over x gives

$$\langle S_y\rangle = \langle\Omega\tau\rangle S_x, \tag{4}$$

which means that large streaming in the x direction implies large streaming in the y direction as well, if one sector dominates.

3. Test particle simulations of neutral sheet diffusion

Building upon the conceptual random sector thickness model introduced in Florinski (2011), we now proceed to investigate the transport of energetic particles across a more realistic representation of magnetic sectors in the heliosheath using a test-particle computer code for orbit integration. Measured plasma velocities are small in the distant heliosheath (Krimigis et al. 2011), and we ignore the background flow altogether. Inside the sectors we assume that the magnetic field $\mathbf{B}$ is constant in magnitude and points either in the $+\hat{\mathbf{z}}$ or the $-\hat{\mathbf{z}}$ directions, corresponding to the primarily azimuthal heliosheath magnetic field. The motion of a charged particle is unrestricted along the field, and we only consider their trajectories in the xy plane (in other words, z is an ignorable coordinate in the present model).

In the computer model used here particles are injected into a two-dimensional rectangular simulations box of size $L_x \times L_y$ containing a few hundred alternating polarity sectors separated by current sheets (which represent different segments of the same HCS). Whereas a theoretical number of sectors in one 11-year solar cycle is about 150, we use a larger number in the model to obtain a correct asymptotic behavior for large times. The current sheets are, on average, parallel to the yz plane, and their mean spacing along the x (radial) direction is d. We introduce perturbations to the form (x-displacement) of each current sheet according to

$$x_s(y) = x_{s0} + \sum_{n=1}^{N_k} A_n \cos(k_n y + \beta_{sn}), \tag{5}$$

where $x_{s0} = sd$ (s is the integer label enumerating the sheets), k_n is the wavenumber of mode n, β_{sn} is the random phase, and A_n is the amplitude, related to the power spectrum of the fluctuations $S(k)$ as (e.g. Giacalone & Jokipii 1999)

$$A_n^2 = \frac{S(k_n)\Delta k_n \sigma_x^2}{\sum_{m=1}^{N_k} S(k_m)\Delta k_m}. \tag{6}$$

The model one-dimensional spectrum of current sheet displacements consists of a flat energy range between $k_{\rm min}$ and k_b, the "bend-over" wave number, followed by an inertial range with $S \sim (k/k_b)^{-5/3}$ extending to $k_{\rm max}$. We use $N_k = 150$ logarithmically equidistant modes separated by Δk_n. For the heliosheath we assume that $k_{\rm max} = 2\pi/0.05\,{\rm AU}^{-1}$ and $k_{\rm min} = 2\pi/79\,{\rm AU}^{-1}$, a difference of 3.2 orders of magnitude, with k_b at the midpoint of the logarithmic interval. This is our "standard" sector boundary displacement structure. From the central limit theorem one may infer that the sector width distribution thus obtained should be Gaussian, with mean d and dispersion σ_x. A direct numerical calculation of the distribution function confirmed that this is indeed the case.

In our simulations length is measured in units of the largest (for pitch angle $\pi/2$) particle gyro-radius $r_g = pc/(ZeB)$, where p is momentum and Z is its charge number. The field is computed on a fine grid with equal mesh spacing in both directions; a typical simulation may contain up to 30 billion grid cells. The $L_x : L_y$ aspect ratio varies depending on the ratio of calculated diffusion coefficients in the two directions, κ_{xx} and κ_{yy} (see below). Typically we set $L_x/L_y \approx (\kappa_{xx}/\kappa_{yy})^{1/2}$. The size of the box is chosen such that no particles escape through any side of the box by the end of the run time. Note that particles traveling the farthest from their starting point contribute the most to diffusive transport statistics at later times. If such particles were allowed to leave the system, the resulting diffusion coefficients would be underestimated. Figure 5 shows a fragment of the sector boundary structure calculated with $d = 1.25 r_g$ and $\sigma_x = 0.3 r_g$. The wiggles in the shape of the sheet are assumed to be a result of turbulent flows in the solar wind and heliosheath that displace the HCS radially.

In our model the sector structure is controlled by three parameters: d, σ_x, and k_b (assuming the ratio $k_{\rm max}/k_{\rm min}$ is a constant). The resulting magnetic field topology may be viewed as a special case of strong "turbulence" with zero mean field. This type of turbulence

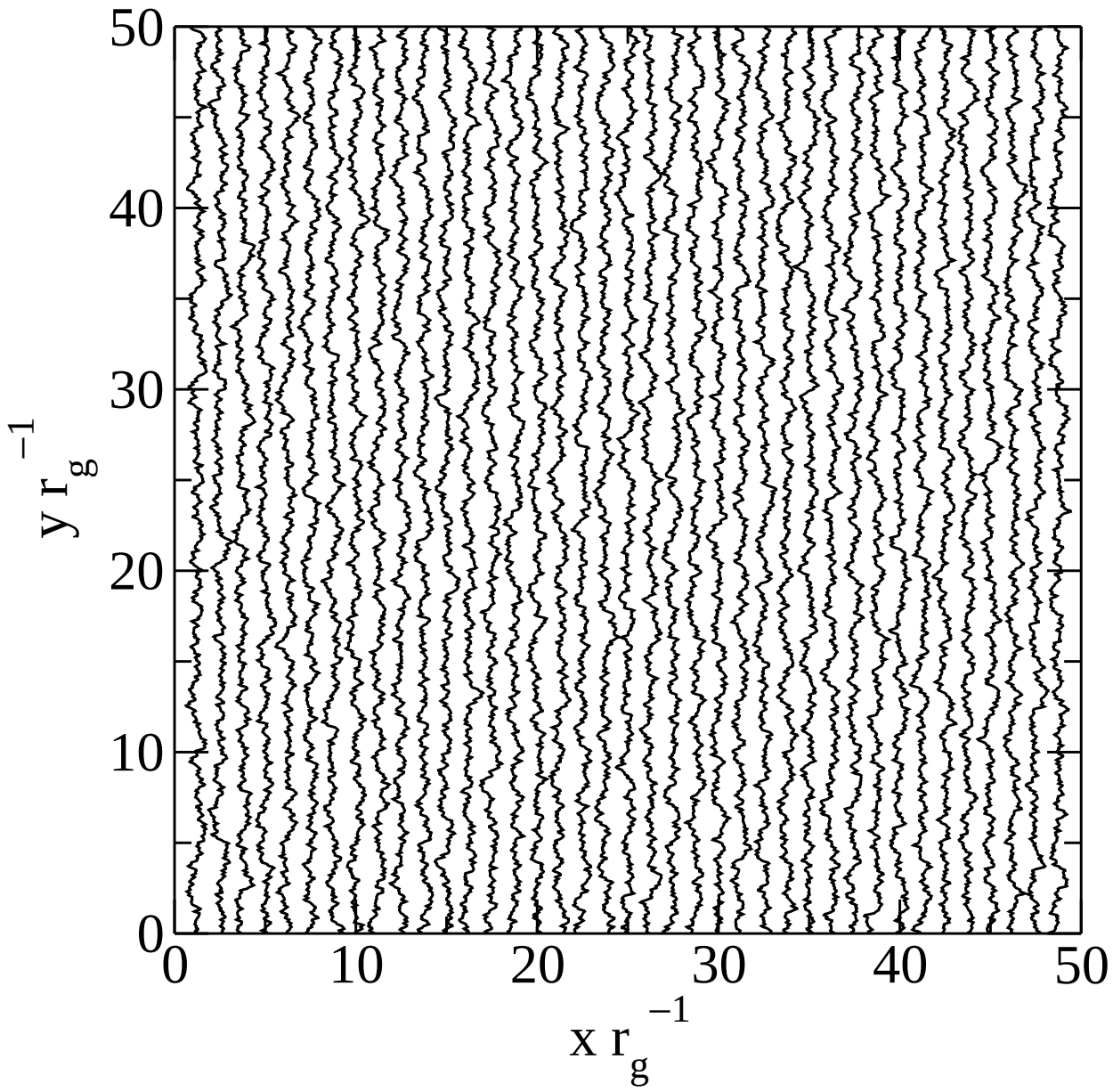

Fig. 5.— Magnetic sector boundaries (a small fragment of the entire simulation) in the xy plane with $d = 1.25r_g$, $\sigma_x = 0.3r_g$, and $k_b = 1.57r_g^{-1}$. The magnetic field is perpendicular to the page.

does not belong to the conventional slab/2D classification system (Matthaeus et al. 1990; Bieber et al. 1996). In our case the fluctuating field $\delta\mathbf{B} \parallel \hat{\mathbf{z}}$ is orthogonal to the plane spanned by the wavevectors (the xy plane). The turbulence is clearly non-axisymmetric; the perpendicular (x) power spectrum is dominated by a signal at π/d (twice the mean current sheet spacing), and the parallel (y) spectrum has no clearly identifiable dominant wavenumber.

Charged particle orbits are computed by integrating the Newton-Lorentz equation of motion

$$\frac{d\mathbf{v}}{dt} = \mathbf{v} \times \mathbf{\Omega}, \tag{7}$$

where $\mathbf{v}$ is the particle's velocity and $\mathbf{\Omega} = Ze\mathbf{B}/(\gamma mc)$ is its cyclotron frequency, m being the mass and γ the relativistic factor. Eq. (7) is solved numerically using the standard fourth-order Runge-Kutta (RK4) method. To achieve good accuracy we used a small time step, typically $\Delta t = 2\pi(1000\Omega)^{-1}$. The spatial resolution in both (x, y) directions was $\Delta x = \Delta y = 0.025 r_g$ (dependent on particle's energy).

Figure 6 illustrates typical particle behavior in a sectored magnetic field with stochastically displaced boundaries. The particle was injected with a fixed pitch angle $\theta = 90^\circ$ near the center of the box. Notice the long excursions in the y direction, corresponding to particle drifting along a single current sheet for long periods of time. The particle may subsequently transfer to an adjacent sheet when the two become sufficiently close. By examining Figure 6 one can envision a certain parallel between particle motion along the current sheets vs. motion across the sectors and motion along and across the mean magnetic field in a conventional slab/2D composite turbulence. Indeed, in the latter case a particle stays on the same field line for a long time, but can at times switch to a different field line as a result of pitch-angle scattering events randomizing its gyrophase. A constriction in the sector structure acts similar to a scattering center allowing a particle to

transfer from one current sheet to another.

From our simulations it emerges that particle transport in both directions becomes diffusive after a certain period of time (dependent on particle's energy, mean sector width, and sector displacement properties). We use running diffusion coefficients calculated as

$$\kappa_{xx}(t) = \frac{\langle [x(t) - x_0]^2 \rangle}{2t}, \quad \kappa_{yy}(t) = \frac{\langle [y(t) - y_0]^2 \rangle}{2t}, \tag{8}$$

where (x_0, y_0) are the initial coordinates of the particles. Here angular brackets mean ensemble averaging over both particles and field realizations. We typically use 25 sector structure realizations and 2000 particles per realization injected in an isotropic shell distribution with a specified kinetic energy T. Figure 7 shows κ_{xx} and κ_{yy} as functions of time for a demonstration run for isotropically injected 200 MeV/n He^{2+} in a field with a strength $B = 0.4$ nT, and the sheet structure as in Fig. 5. The size of the simulation box was 107 AU by 573 AU in the x and y directions, respectively. Such a large size was chosen to ensure that we measure correct asymptotic values of the running diffusion coefficients (see discussion above). All 50,000 particles remained inside the box after 2000 gyro-periods.

After a brief superdiffusive phase, lasting a few tens of gyro-periods, when particles are streaming primarily along individual neutral sheets (marked by increasing $\kappa(t)$), normal diffusion is established in both directions. Asymptotic values of κ_{xx} and κ_{yy} are obtained from this late phase of the particles' trajectories. For the present choice of parameters, the cross-sector diffusion coefficient is a factor of ~ 4 smaller than the "parallel" diffusion coefficient. The ratio κ_{xx}/κ_{yy} depends sensitively on the width of the sectors. The next section demonstrates the dependence of diffusion coefficients on particle's energy and on the properties of current-sheet "turbulence".

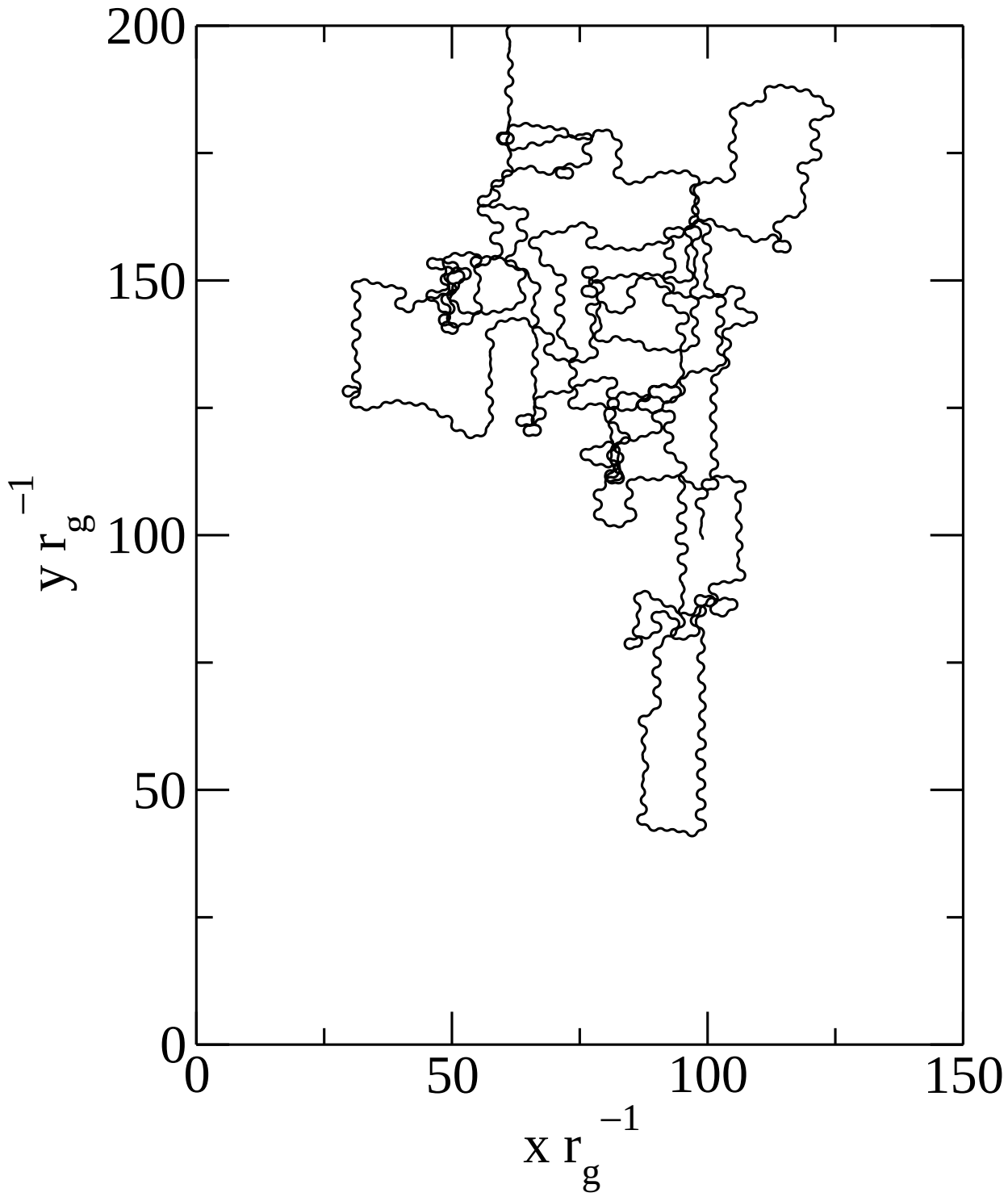

Fig. 6.— A sample charged particle trajectory in a sectored magnetic field with $d = 1.25r_g$, $\sigma_x = 0.3r_g$, and $k_{\rm min} = 1.57r_g^{-1}$, illustrating parallel and perpendicular current sheet transport.

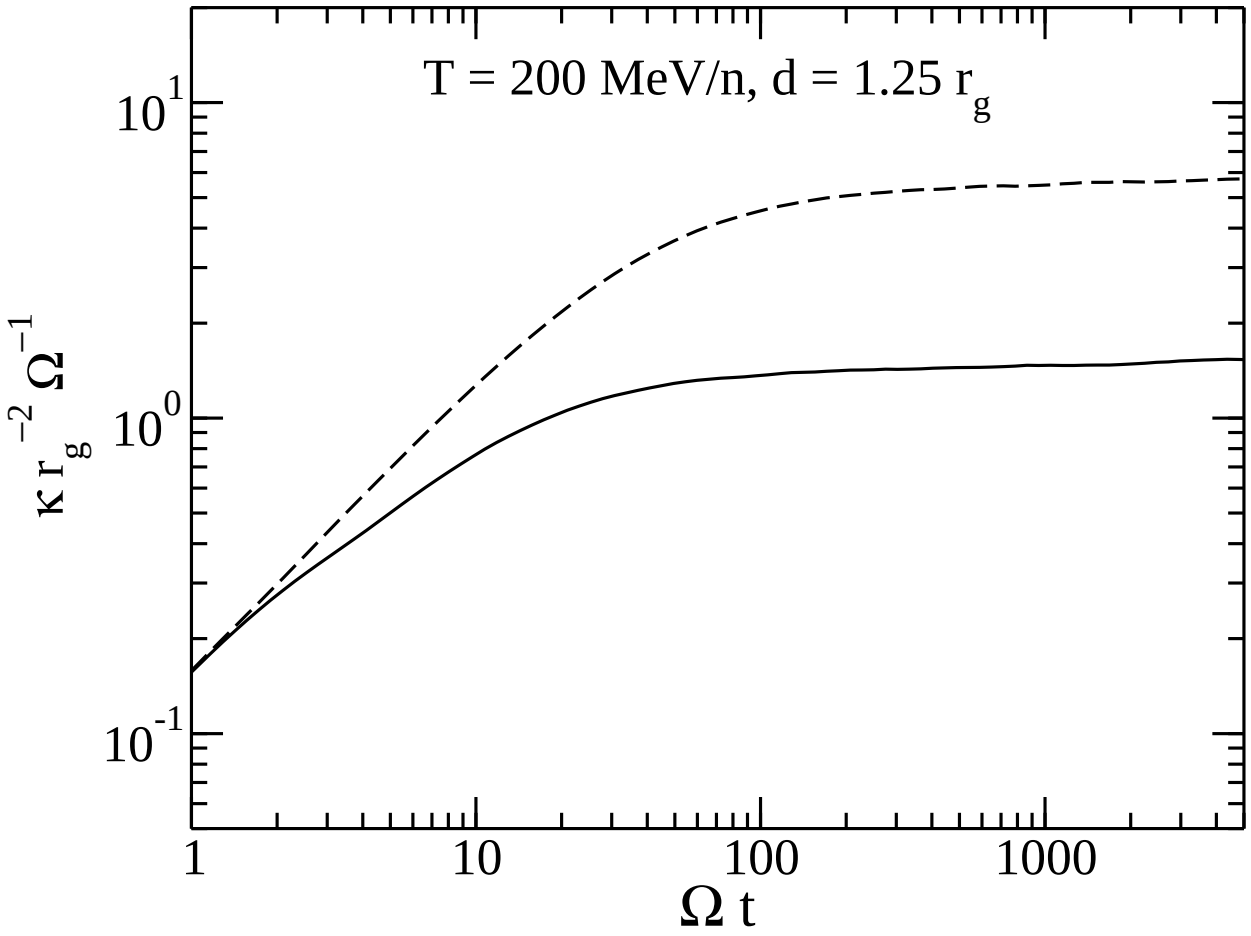

Fig. 7.— Running diffusion coefficients, in units of $r_g^2\Omega$, as a function of time. Isotropically injected 200 MeV/n helium ions in a 4 μG magnetic field, mean sector width $d = 0.062$ AU.

4. Dependence on sector properties and particle energy

We first discuss the dependence of diffusion coefficients on energy. In the following numerical experiments the current sheets had the same properties using the "standard" choice of parameters B, d, σ_x, $k_{\min}$, k_b, and $k_{\max}$ as described in the previous section. The energy of He^{2+} ions was varied between 10 MeV/n and 1 GeV/n. The size of the simulation box was adjusted accordingly to prevent particles from leaving.

The results of this experiment are shown in Figure 8. At the lowest energy (10 MeV/n) the Larmor radius is about 4 times smaller than the mean distance between the sheets and perpendicular diffusion is strongly suppressed. Parallel transport still appears to be super-diffusive by the end of the simulation, which may explain the upturn in κ_{yy} at low energies. By about 100 MeV/n the neutral sheet separation is about equal the Larmor radius leading to a dramatic increase in κ_{xx}. Here transport is strictly diffusive and both coefficients increase with ion energy. The parallel diffusion coefficient is well approximated by a power-law with an index of 3/2, while the perpendicular coefficient increases somewhat faster as $\sim T^2$. In the non-relativistic regime, this behavior is comparable with a quasi-linear theory result $\kappa_{yy} \sim T^{1+\alpha/2}$ for a turbulent power-law spectral slope $\alpha = 1$ (e.g., Jokipii 1971). It is not clear whether there is a connection between the two or it is a simple coincidence. Note that in our model the spectrum of fluctuations in the current sheets varies between $-5/3$ and zero.

Figure 9 shows the dependence of κ_{xx}/κ_{yy} on ion energy. The ratio is a rapidly increasing function of energy ($\sim T^3$ at low energy) and approaches a unity (isotropic diffusion) at high energy. The transition from slow to fast perpendicular diffusion occurs at $r_g \simeq d$.

In the second set of numerical experiments we simulated particles at two fixed energies, 50 MeV/n and 250 MeV/n, while varying the distance d between the sheets and

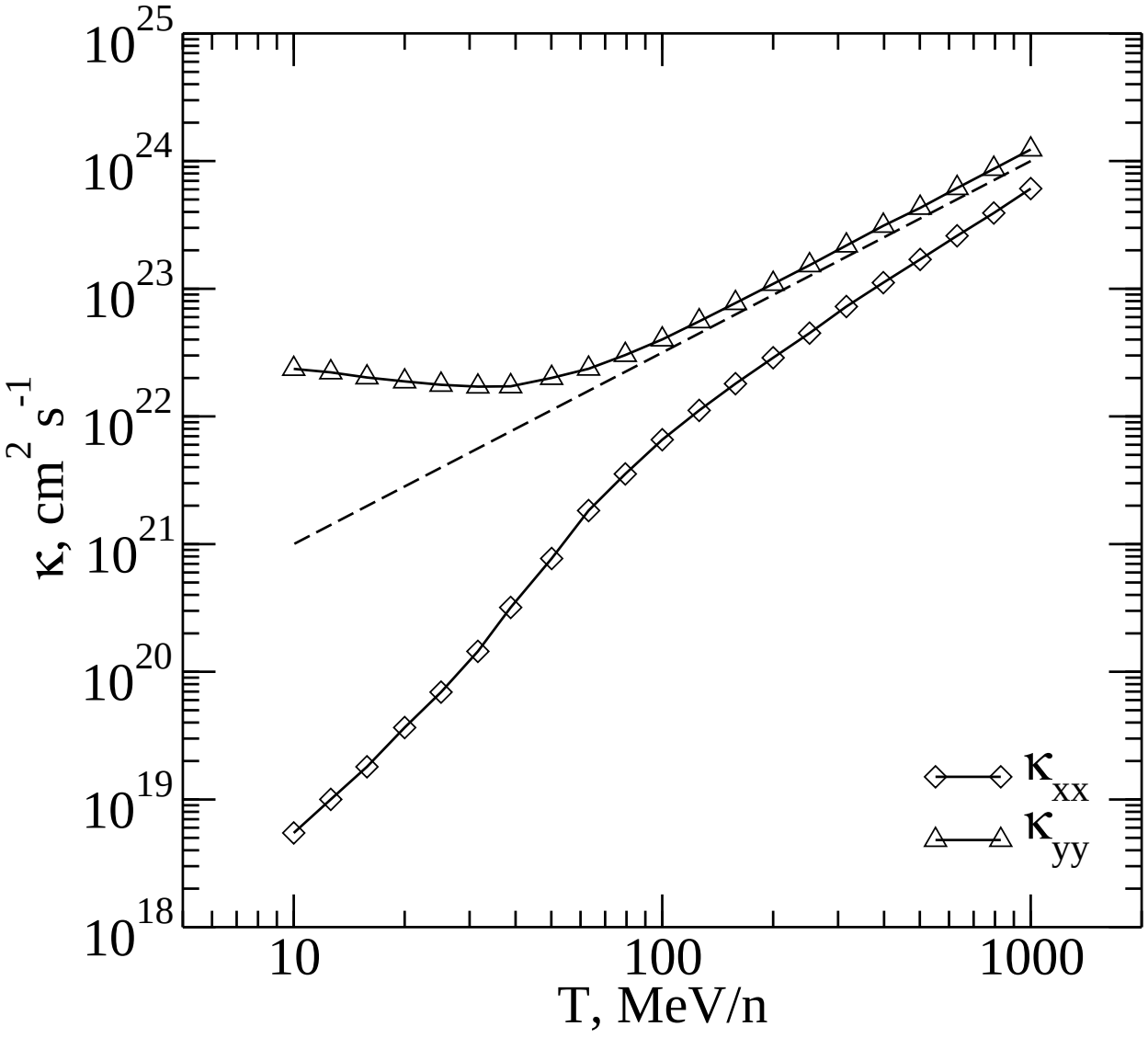

Fig. 8.— Parallel (κ_{yy}) and perpendicular (κ_{xx}) diffusion coefficients for galactic He as a function of energy per nucleon. The dashed line has a power law slope of 3/2.

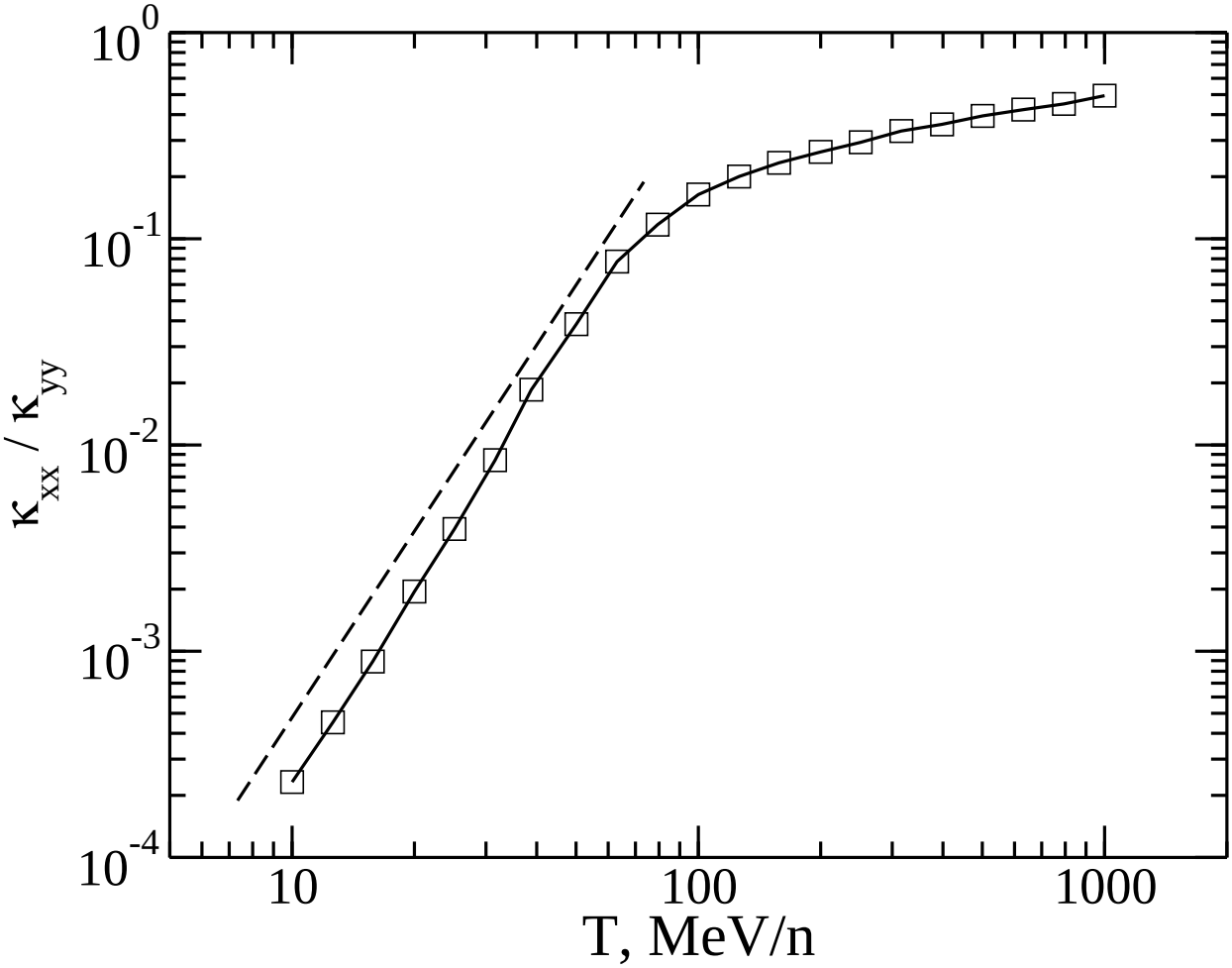

Fig. 9.— Ratio of perpendicular (κ_{xx}) to parallel (κ_{yy}) diffusion coefficients for galactic He as a function of energy per nucleon. The dashed line has a slope of 3.

the displacement magnitude σ_x while keeping the ratio σ_x/d a constant (= 0.24). This approximates a situation where the stack of sectors is compressed, but the wiggles become smaller as well (the complete structure is flattened on approach to the stagnation point). The magnitude of **B** was kept a constant implying that the excess field was removed from the region by a latitudinal flow. The current sheet turbulence spectrum was again of the "standard" type (described following Eq. (6)).

We show the ratio κ_{xx}/κ_{yy} in Figure 10. For 50 MeV/n ions the ratio drops rapidly as the distance d becomes larger than the gyro-radius. Conversely, at 250 MeV/n the decrease is much more gradual. The main reason for this difference is the fact that the power spectrum of neutral sheet oscillations is the same in both simulations (with 50 MeV/n and 250 MeV/n). The two would be alike only if the neutral sheet displacement wavelengths were also varied $\sim d$.

In the final experiment we vary the turbulence spectrum for a fixed energy (100 MeV/n) and sector width ($d = 1.25 r_g$). Instead of a broadband spectrum employed in the previous simulations, here we use a narrow-band spectrum with a constant power spectral density between $k_{\rm min}$ and $k_{\rm max}$. The spectrum extends a single decade in wavenumber and is represented with $N_k = 50$ modes. Running diffusion coefficients at the end of each run are recorded as the asymptotic values.

The results are plotted in Figure 11. We see that increasing the wavelength leads to an increase in κ_{yy} and a decrease in κ_{xx}. The latter is easily understood from the fact that by reducing $k_{\rm min}$ the mean distance between neutral sheet constrictions, acting as scattering centers, increases leading to a reduction in scattering rates. There is a rapid drop in κ_{yy} near what could be described as "resonant" wavenumber where kr_g is of order 1. It is not clear what causes the upturn at large $k_{\rm min}$. It is conceivable that the model is unable to resolve such fine structures with good accuracy.

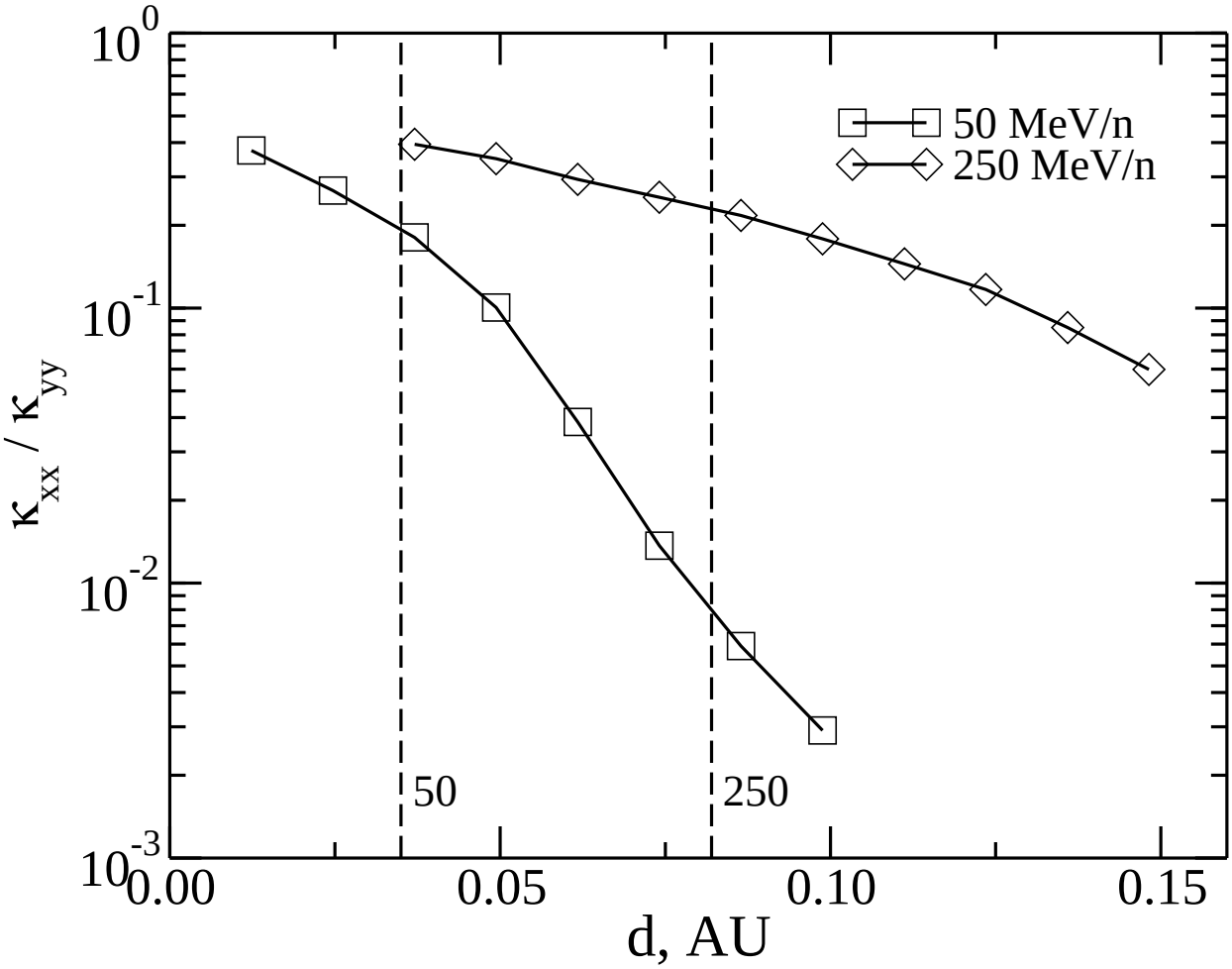

Fig. 10.— Ratio of perpendicular (κ_{xx}) to parallel (κ_{yy}) diffusion coefficients at 50 MeV/n (squares) and 250 MeV/n (diamonds) as a function of mean sector thickness. The ratio of the magnitude of sector boundary fluctuations and the sector thickness was kept a constant (0.24). Vertical dashed lines are the gyro-radii of both ions in a 0.4 nT magnetic field.

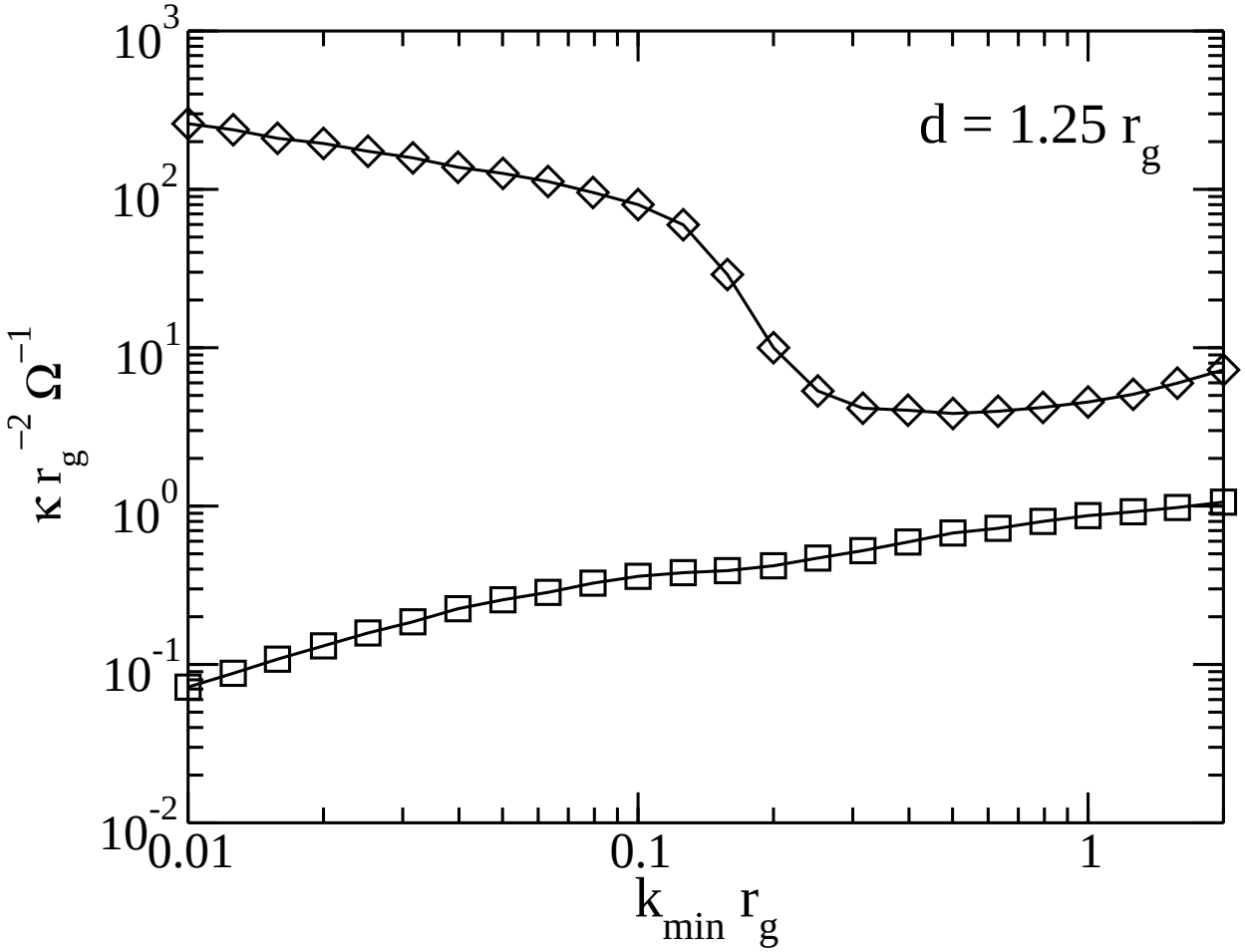

Fig. 11.— Parallel (κ_{yy}, diamonds) and perpendicular (κ_{xx}, squares) diffusion coefficients of 100 MeV/n He ions as a function of $k_{\rm min}$. The wavenumber and the diffusion coefficients are normalized to r_g and $r_g^2\Omega$, respectively. The mean sector width $d = 1.25 r_g$.

5. Discussion

Analytic and numerical results presented here clearly demonstrate that a warped HCS can facilitate charged particle transport perpendicular to the mean magnetic field, if the distance between the folds d is comparable to (or smaller than) the particle's Larmor radius, the condition that is expected to be satisfied within about 10 AU before the heliopause. The analytic treatment of the problem was performed using the Boltzmann equation for a non-gyrotropic velocity distribution. Unlike the numerical model, the sector width was constant. Instead, stochasticity was provided by small-angle gyrophase scattering events. Our results show a steady increase in the cosmic-ray differential current perpendicular to the sectors (and therefore, in the cross-field diffusion coefficient) with the ratio r_g/d. Gyration can produce net streaming along the sector planes if the widths of the positive and the negative sectors are different. The magnitude of the streaming flux tends to increase with r_g/d.

In our test-particle simulations we found that particles undergo diffusive random walk in the plane perpendicular to $\mathbf{B}$, i.e., in the radial and latitudinal directions. The efficiency of this process depends critically on the size of neutral sheet "wiggles" and the mean thickness of the alternating polarity sectors. The ratio of perpendicular and parallel diffusion coefficients is zero in the limit of very long-wavelenfth fluctuations, and when the ratio r_g/d is small. In the opposite limit (short-wavelength fluctuations, $r_g/d > 1$) the ratio approaches unity. In the latter regime, the value of κ_{rr} could be as large as $6 \times 10^{21} - 6 \times 10^{23}$ cm^2/s for He^{2+} ions with energies between 100 MeV and 1 GeV per nucleon, assuming a magnetic field strength of 0.4 nT (see Figure 8). These values are larger than the perpendicular diffusion coefficients calculated using the standard theory for solar-wind fluctuations. For example, in the model of Florinski & Pogorelov (2009) $\kappa_\perp$ is between 4×10^{21} and 4×10^{22} cm^2/s for 100 MeV and 1 GeV protons, respectively.

For helium with the same energy per nucleon the diffusion coefficients will be larger by up to a factor of 4 (for resonant interactions in the energy range of the turbulence with $\kappa_\parallel \sim r_g^2$ and $\kappa_\perp \sim \kappa_\parallel$). The current-sheet radial diffusion coefficient is about a factor of 5 larger. Remember, however, that conventional scattering by turbulence was not included in our model. We expect our results to be more reliable in a situation where the level of background turbulent activity at resonant wavenumbers is relatively low.

The interplay between the sheet-parallel and perpendicular transport in our model resembles in several ways conventional diffusion along and across the magnetic field. Constrictions between the adjacent sheets appear to play the role of scattering centers. Nevertheless, one should exercise caution before drawing parallels between the two. Parallel diffusion in QLT is a resonant process, which is clearly not the case for current sheet diffusion.

The current sheet transport mechanism is most efficient for galactic ions with energies of the order 100 MeV per nucleon and above. Voyager 1 observations of galactic helium made near the end of 2011 at a heliocentric distance of ~ 119 AU (McDonald et al., AGU abstract) are close or in excess of the predicted interstellar intensities from Webber & Higbie (2009). If Voyager 1 is 10 AU in front of the heliopause, the current-sheet effect could be responsible for the lack of modulation. Another possible cause is the absence of a radial plasma flow (Krimigis et al. 2011) which would otherwise expel energetic particles from the heliosheath.

The diffusion mechanism discussed here may facilitate the transport of interstellar dust grains with size < 0.01 μm that have a gyroradius similar to that of a few hundred MeV cosmic-ray ion (Czechowski & Mann 2003). Conversely, it is not efficient for low-rigidity particles such as electrons, because their gyro-radius is much smaller than the distance between the adjacent sheets. The recent rise of the low-energy electrons measured by the

Voyagers (Caballero-Lopez et al. 2010; Webber et al. 2012), is probably not directly related to the current sheet diffusion effect discussed here. At such small rigidities the effect of magnetic field meandering is likely to take precedence over current sheet transport as described by our current model. The model is somewhat restricted by the assumption that the direction along $\mathbf{B}$ is an ignorable coordinate; this could lead to an under-estimate of the diffusion rate in the radial direction.

We realize that a more accurate diffusion model should include "conventional" turbulence (variations in the magnitude and direction of $\mathbf{B}$) in addition to the current-sheet oscillations. Such a project would require massively larger computer simulations taking thousands of CPU-hours for a single run, but may be ultimately needed solve the problem of cosmic-ray transport in the distant heliosheath. Despite technical difficulties, in the future it might be possible to combine the two kinds of diffusion into a single three-dimensional model of energetic charged particle transport.

V.F. was supported, in part, by NASA grant NNX10AE46G, NSF grant AGS-0955700 (also supporting X.G.) and by a cooperative agreement with NASA Marshall Space Flight Center. J.K. acknowledges support by NASA grant NNX08AQ14G.

REFERENCES

Achatz, U., Steinacker, J., & Schlickeiser, R. 1991, A&A, 250, 266

Bieber, J. W., Wanner, W., & Matthaeus, W. H. 1996, J. Geophys. Res., 101, 2511

Borovikov, S. N., Pogorelov, N. V., Burlaga, L. F., & Richardson, J. D. 2011, ApJ, 728, L21

Burlaga, L. F., & Ness, N. F. 2010, ApJ, 725, 1306

Burlaga, L. F., Ness, N. F., & Richardson, J. D. 2003, J. Geophys. Res., 108, 8028

Caballero-Lopez, R. A., Moraal, H., & McDonald, F. B. 2010, ApJ, 725, 121

Czechowski, A., & Mann, I. 2003, J. Geophys. Res., 108, 8038

Czechowski, A., Strumik, M., Grygorczuk, J., Grzedzielski, S., Ratkiewicz, R., & Scherer, K. 2010, A&A, 516, A17

Earl, J. A, Jokipii, J. R., & Morfill, G. 1988, ApJ, 331, L91

Florinski, V. 2011, Adv. Space Res., 48, 308

Florinski, V., & Pogorelov, N. V. 2009, ApJ, 701, 642

Giacalone, J., & Jokipii, J. R. 1999, ApJ, 520, 204

Intriligator, D. S., Sun, W., Dryer, M., Fry, C. D., Deehr, C., & Intriligator, J. 2005, J. Geophys. Res., 110, A09S10

Jokipii, J. R. 1971, Rev. Geophys. Space Phys., 9, 27

Kóta, J. 1975, J. Phys. A, 8, 1349

Krimigis, S. M., Roelof, E. C., Decker, R. B., & Hill, M. E. 2011, Nature, 474, 359

Mace, R. L., Matthaeus, W. H., & Bieber, J. W. 2000, ApJ, 538, 192

Matthaeus, W. H., Goldstein, M. L., & Roberts, D. A. 1990, J. Geophys. Res., 95, 20,673

Morfill, G. E., and Grün, E. 1979, Planet. Space Sci., 27, 1283

Parker, E. N. 1965, Planet. Space Sci., 13, 9

Qin, G., Matthaeus, W. H., & Bieber, J. W. 2002, ApJ, 758, L117

Richardson, J. D., Stone, E. C., Kasper, J. C., Belcher, J. W., & Decker, R. B. 2009, Geophys. Res. Lett., 36, L10102

Richardson, J. D., & Wang, C. 2011, ApJ, 734, L21

Riley, P., Linker, J. A., & Mikić, Z. 2002, J. Geophys. Res., 107, 1136

Webber, W. R., & Higbie, P. R. 2009, J. Geophys. Res., 114, A02103

Webber, W. R., McDonald, F. B., Cummings, A. C., Stone, E. C., Heikkila, B., and Lal, N. 2012, Geophys. Res. Lett., 39, L06107